Atomistic study of the migration of di- and tri-interstitials in silicon

M. Posselt,[1,*] F. Gao,[2] and D. Zwicker[1]
[1]*Forschungszentrum Rossendorf, Institute of Ion Beam Physics and Materials Research, P. O. Box 510119, D-01314 Dresden, Germany*
[2]*Pacific Northwest National Laboratory, Fundamental Science Directorate, P. O. Box 999, Richland, Washington 99352, USA*
(Received 11 January 2005; published 22 June 2005)

A comprehensive study on the migration of di- and tri-interstitials in silicon is performed using classical molecular dynamics simulations with the Stillinger-Weber potential. At first the structure and energetics of the di- and the tri-interstitial are investigated, and the accuracy of the interatomic potential is tested by comparing the results with literature data obtained by tight-binding and density-functional-theory calculations. Then the migration is investigated for temperatures between 800 and 1600 K. Very long simulation times, large computational cells and different initial conditions are considered. The defect diffusivity, the self-diffusion coefficient per defect and the corresponding effective migration barriers are calculated. Compared to the mono-interstitial, the di-interstitial migrates faster, whereas the tri-interstitial diffuses slower. The mobility of the di- and the mono-interstitial is higher than the mobility of the lattice atoms during the diffusion of these defects. On the other hand, the tri-interstitial mobility is lower than the corresponding atomic mobility. The migration mechanism of the di-interstitial shows a pronounced dependence on the temperature. At low temperature a high mobility on zig-zag-like lines along a ⟨110⟩ axis within a {110} plane is found, whereas the change between equivalent ⟨110⟩ directions or equivalent {110} planes occurs seldom and requires a long time. At high temperature a frequent change between equivalent ⟨110⟩ directions or {110} planes is observed. During the diffusion within {110} planes the di-interstitial moves like a wave packet so that the atomic mobility is lower than that of the defect. On the other hand, the change between equivalent {110} migration planes is characterized by frequent atomic rearrangements. The visual analysis of the tri-interstitial diffusion reveals complex migration mechanisms and a high atomic mobility. The diffusivities and effective migration barriers obtained are compared with the few data from the literature. The implications of the present results for the explanation of experimental data on defect evolution and migration are discussed.

DOI: 10.1103/PhysRevB.71.245202 PACS number(s): 61.72.Bb, 61.72.Ji, 85.40.Ry, 61.80.Az

I. INTRODUCTION

Small self-interstitial clusters play an important role in the current understanding of defect evolution and transient-enhanced diffusion of boron during post-implantation annealing.[1–3] These clusters are assumed to be formed as a transient storage of self-interstitials during an Ostwald ripening process. According to this model the self-interstitial exchange between the clusters is due to diffusing mono-interstitials whereas the clusters themselves are immobile. The ripening and dissolution of the clusters determine the time scale for the supersaturation of mono-interstitials and therefore the time constant of the transient-enhanced boron diffusion. Furthermore, clusters formed by boron and self-interstitials as well as the influence of impurities have to be considered in order to explain the experimental results satisfactorily.

The structure and energetics of small self-interstitial clusters have been investigated by different computational methods.[4–16] Recently, some theoretical studies indicated that besides the mono-interstitial the di- and the tri-interstitial are mobile as well.[4,5,7,17–20] This may lead to a revision of the current understanding of the results of many experiments performed in the last decade, amongst them those on defect evolution and transient-enhanced diffusion of boron. On the other hand, the previous knowledge on the migration of di- and tri-interstitials is still limited and only a few systematic investigations have been carried out. In this work a comprehensive atomistic study is performed in order to get a better understanding of the mechanisms of di- and tri-interstitial diffusion at different temperatures and to obtain more data for their diffusivities and migration barriers. A classical potential approach is employed since it allows the investigation of defect migration under relatively realistic conditions, by considering a large computational cell, a very long simulation time, and different initial conditions. The accuracy of the interatomic potential used in such molecular dynamics (MD) simulations determines decisively the reliability of the results. In order to test the potential employed, in the first part of this work the structure and energetics of di- and tri-interstitials are investigated and the results are compared with the data obtained by tight-binding calculations and the density-functional theory, which consider both the ionic and the electronic degrees of freedom. The main part of the present work deals with the classical MD simulations of di- and tri-interstitial diffusion. Although their computing time is still considerable, it is much smaller than for MD simulations based on the more sophisticated methods. Systematic MD simulations based on the density-functional theory are presently not practicable since they require a tremendous computational effort. An alternative to MD simulations is the estimation of migration barriers using the potential energy surface at 0 K, which can be calculated by a classical potential approach, by the tight-binding method or by the density-functional theory. However, the determination of the barriers is a difficult task since the di- and the tri-interstitials have rather complex structures. Furthermore, the migration barriers may change with temperature, so that the proposed

method may not lead to correct results. The results of the comprehensive atomistic study on the migration of di- and tri-interstitials are compared with the few theoretical data obtained by other authors. Finally, a detailed discussion is performed about the implications of the present results for the explanation of experiments on post-implantation annealing and on room-temperature migration of implantation-induced self-interstitial defects.

II. SIMULATION METHOD

In the present work the modified Stillinger-Weber (SW) potential[21,22] is employed. The modification consists solely in the multiplication of the original two- and three-body energy parameters by a factor of about 1.07 in order to obtain the correct value for the cohesive energy.[22] Together with the Tersoff 3 potential,[23] the SW potential is the most commonly used interatomic potential for silicon, and its features have been extensively studied. In view of the subject of the present work, the SW potential is chosen for the following reasons. It gives a reasonable description of many static and dynamic properties of the silicon lattice and the melting temperature agrees well with the experimental value.[22,24,25] The SW potential yields a $\langle 110 \rangle$ dumbbell configuration as the most stable mono-interstitial[26] and an inwards relaxation of the atoms around the mono-vacancy.[22] This is in agreement with the results of many density-functional-theory calculations.[27–29] However, in the case of the SW potential two $\langle 110 \rangle$ dumbbell structures are found, namely the normal and the extended dumbbell.[26] The latter is most stable, the former has the second lowest formation energy. On the other hand, the Tersoff 3 potential yields the tetrahedral configuration as the most stable mono-interstitial and an outwards relaxation[22] of the atoms around the mono-vacancy. Furthermore, the Tersoff 3 potential gives a wrong melting temperature.[5,22,24,30,31] The SW potential has a number of shortcomings[15,32] as well. Therefore, it has been checked whether the recently developed potentials of Justo *et al.*[32] and Lenosky *et al.*[15] should be employed. However, in the case of the Lenosky potential two tetrahedral configurations are the most stable mono-interstitials and the melting point is too low.[15] The melting temperature obtained by the Justo potential is lower than the experimental value, but higher than that for the Lenosky potential.[32] It yields the $\langle 110 \rangle$ dumbbell as the most stable mono-interstitial. For present investigations, the Justo potential may be therefore an alternative to the SW potential.

The simulation cell is a cube-like rectangular parallelepiped with *x*-, *y*-, and *z*-directions parallel to the $[-110]$, $[-1\,-12]$, and $[111]$ axes, respectively. Three-dimensional periodic boundary conditions are applied. In order to minimize the interaction of the di- and tri-interstitials with their periodic replicas, relatively large simulation cells are used. They consist of $1008+2$ and $2880+3$ atoms in the di- and tri-interstitial studies, respectively. In some cases even larger simulation cells are used in order to estimate the influence of the cell size on the simulation results.

The search for defect structures with the lowest formation energies is conducted employing a procedure similar to the "scrambled relaxation" method.[6] At first two or three extra atoms are introduced into the perfect crystal in a suitable manner. In investigations of di-interstitials, typical start configurations are two neighboring (unrelaxed) $\langle 110 \rangle$ dumbbells or a tetrahedral interstitial adjacent to a $\langle 110 \rangle$ dumbbell. A characteristic structure used as start configuration for tri-interstitial simulations consists of two $\langle 110 \rangle$ dumbbells at the same lattice site but with different orientations. In a second step, all atoms in the simulation cell are randomly displaced along the *x*-, *y*-, and *z*-directions using an uniform distribution of the displacements with a cutoff of ±0.5 Å. Finally, the system is relaxed to 0 K by applying a rapid quenching scheme that is based on MD simulations. It should be noted that the method described above does not necessarily yield the complete defect hierarchy (including the metastable defect states) since it is based on a heuristic approach for searching the most stable di- and tri-interstitial configurations. Unfortunately, a rigorous method to obtain the complete defect hierarchy does not exist.

The investigations of defect migration start with a simulation cell at 0 K, containing one of the di- or tri-interstitial configurations with the lowest formation energies. Then, the atoms of the outermost layer of the cell are coupled to a heat bath. In order to avoid the dissociation of the di- or tri-interstitial, the temperature is gently increased using a Berendsen heater[33] with a relaxation time of 10 ps. The heat bath is maintained throughout the migration simulation. The thermal expansion of the perfect crystal is taken into account, i.e., a $N, V(T), T$ system is considered. In the temperature range considered in the this work, the value of the linear thermal expansion coefficient derived using the SW potential $(4\times10^{-6}\ \mathrm{K}^{-1})$ agrees well with the experimental data.[34] After heating up the system to the diffusion temperature, the migration of the di- and the tri-interstitial and of the Si atoms is followed for different periods. The lower the temperature, the longer is the simulation time. The atomic mobility due to the presence of the di- or tri-interstitial is characterized by the time dependence of the sum of the squared displacements ssd_a of all atoms

$$\mathrm{ssd}_a(t) = \sum_{i=1}^{N} (\mathbf{r}_i(t) - \mathbf{r}_i(0))^2,$$

where $\mathbf{r}_i(0)$ is the position of atom i at the beginning of the migration simulation, and $\mathbf{r}_i(t)$ is the position at time t. N denotes the total number of atoms in the simulation cell. The self-diffusion coefficient per di- or tri-interstitial (D_s) is obtained by fitting $\mathrm{ssd}_a(t)$ to a linear expression and by employing the Einstein relation[4,35]

$$\mathrm{ssd}_a(t) = \mathrm{const.} + 6D_s t.$$

The constant corresponds to the sum of the squared displacements of the atoms in the perfect crystal at the given temperature.

The diffusivity D_d of the di- or tri-interstitial is calculated in the following manner. Throughout the migration simulation, the defect configuration is monitored by analyzing the Wigner-Seitz cells of the perfect lattice. The criterion for

interstitial identification is the existence of more than one atom in the same cell. Based on the Wigner-Seitz cell analysis, the trajectory of the center of mass of the di- or tri-interstitial is determined.[35–37] In order to obtain the diffusivity of the defect, the trajectory is decomposed into time segments,[35,36,38] and for each segment m the squared displacement sd_d of the center of mass $\mathbf{R}(t)$ of the defect is calculated: $\mathrm{sd}_d(m)=(\mathbf{R}(t_m)-\mathbf{R}(t_{m-1}))^2$, $t_m=t_{m-1}+\Delta t$. Applying the Einstein relation and averaging over all segments n_s leads to the defect diffusion coefficient

$$D_d=\frac{1}{n_s}\sum_{i=1}^{n_s}\frac{\mathrm{sd}_d(m)}{6\Delta t}.$$

Within certain limits, the number (or the size) of the time intervals can be chosen arbitrarily.[35,36,38] Therefore, a further averaging can be performed over all possible decompositions. In this manner, an improvement of the statistical accuracy of the result is possible. Additionally to the calculation of diffusion coefficients, the atomic mechanisms of the migration of di- and tri-interstitials are investigated. For this purpose, the defect trajectories and the atomic rearrangements during the defect migration are analyzed. It is also checked whether a dissociation of the di- or tri-interstitials occurs since this case has to be excluded from the present considerations. For comparison, the diffusion of mono-interstitials is investigated as well, employing similar methods as described for di- and tri-interstitials.

III. RESULTS AND DISCUSSION

A. Structure and energetics of di- and tri-interstitials

The search procedure described in the previous section was applied several hundred times, using different random atomic displacements at the start of the relaxation step. The most stable di- and tri-interstitial configurations found by this method are depicted in Figs. 1 and 2, respectively. Their formation and binding energies are given in Table I. The binding energy is defined as the energy required to split up an interstitial cluster into well-separated (i.e., noninteracting) mono-interstitials with a formation energy of 3.92 eV. This is the value for the extended $\langle 110\rangle$ dumbbell, the most stable mono-interstitial configuration in the Stillinger-Weber silicon. The di-interstitial with the lowest formation energy is the "Z structure" which consists of two neighboring $\langle 110\rangle$ dumbbells in the same $\{110\}$ plane. The "modified tetrahedron" is the most stable tri-interstitial, where two $\langle 110\rangle$ dumbbells in perpendicular $\{110\}$ planes share the same lattice site. Since the search method employed does not necessarily yield the complete defect hierarchy (including the metastable states), the present results should be considered with some caution. The defect structures found are relatively compact structures. Noncompact configurations with low formation energies, consisting of interacting mono- and di-interstitials, may also exist. The influence of the size of the simulation cell on the results on the structure and the energetics of di- and tri-interstitials was estimated. Using a cell of $2880+2$ atoms for the di-interstitial, and a cell of $5040+3$ atoms for the tri-interstitial, led to the same defect hierarchy as for the standard cell size. The corresponding formation energies differ by less than 0.5%.

For comparison, Table I shows results of other theoretical investigations on the structure and energetics of di- and tri-interstitials. They were determined using classical potential methods, tight-binding calculations, and the density-functional theory. Different approaches were employed in order to find the most stable di- and tri-interstitial configurations. The methods of Rasband *et al.*[6] and Bongiorno *et al.*[8] are similar to that used in the present work. Richie *et al.*[13] applied the density-functional theory to analyze various di- and tri-interstitial structures found during long-time tight-binding simulations at different temperatures. Defect configurations identical or similar to those depicted in Figs. 1 and 2 were also found by the other authors. Some authors reported defect structures which were not obtained by the present investigations. The formation energies of the di-interstitials I_2^A and I_2^B are close to the values determined by most recent density-functional theory calculations.[13] However, one di-interstitial configuration with a lower formation energy than for I_2^A was obtained by these authors. The tri-interstial configurations I_3^A, I_3^B, and I_3^C are similar to the "tetrahedron" and the "bond-centered triple" found by the other authors. Their formation energies agree fairly well with the results of most recent density-functional calculations.[13,14] In Ref. 13, a rather complex tri-interstitial with a lower formation energy than for the "tetrahedron" was detected. The comparison of all data determined by density-functional-theory studies does not lead to a unique picture. The lowest formation energies obtained for di- and tri-interstitials vary between 4.9 and 6 eV, and between 6.0 and 7.3 eV, respectively. The corresponding tight-binding data for the di-interstitial lie between 4.9 and 7.3 eV, for the tri-interstitial between 6.7 and 7.8 eV. Classical potential methods yielded values between 5.7 and 6.3 eV for the di-interstitial and 6.0–8.8 eV for the tri-interstitial. It is remarkable that the formation energies determined by rather different theoretical methods vary within a similar range. The data on the structure and energetics of di- and tri-interstitials obtained by the Stillinger-Weber potential are comparable with those determined by the more sophisticated methods.

The results of the theoretical investigations were related to experimental data obtained by electron paramagnetic resonance (EPR), photoluminescence (PL) spectroscopy and other methods.[9,10,40,41] Some authors found that the P6 EPR center is due to the di-interstitial[9,40,41] and the PL W center is caused by the tri-interstitial.[10] However, the relation of these spectroscopic data to the di- and the tri-interstitials was questioned by Jones *et al.*[10] and Lopez *et al.*,[14] respectively. On the other hand, di- and tri-interstitials as well as larger self-interstitial clusters were postulated as transient defect states in order to explain the defect evolution and the transient-enhanced boron diffusion during post-implantation annealing.[1–3]

B. Diffusion of di- and tri-interstitials

The migration of di-interstitials was investigated at 800, 1000, 1200, 1400, and 1600 K. At each temperature, the

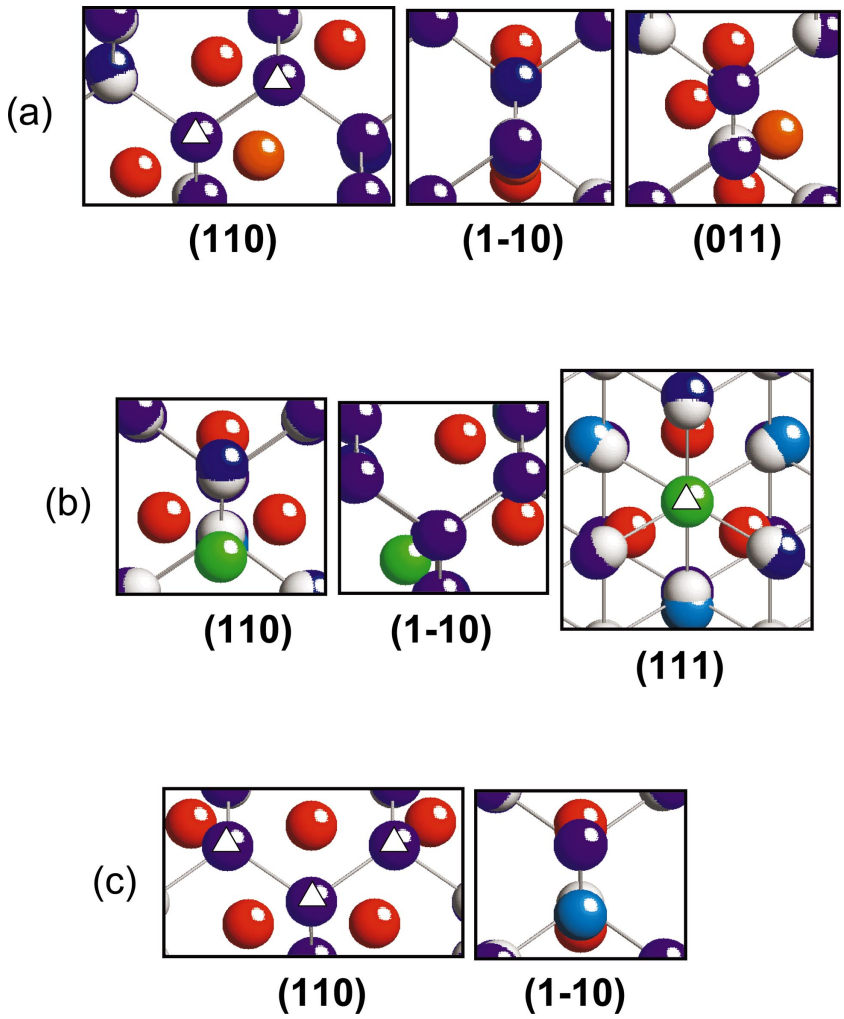

FIG. 1. (Color) The three di-interstitial configurations with the lowest formation energies: I_2^A (a), I_2^B (b), and I_2^C (c). Views on different crystallographic planes illustrate the spatial structure of the defects. The light gray spheres and cylinders depict atoms and bonds of the ideal lattice. The colored spheres show the atoms in the real lattice, including those belonging to the di-interstitial. The color is a measure for the deviation of atomic positions from the ideal lattice sites. Red and blue color mean large and small deviations, respectively. The values of the formation energies of the shown di-interstitials are given in Table I. Note, that in the views onto the (110) plane in (a) and (c), and in the view onto (111) in (b), the figure plane is parallel to the plane where the di-interstitial is situated, but not identical to this plane. Therefore, the lattice sites from which atoms of the di-interstitial come are hidden by other atoms of the real lattice. These sites are marked by the white triangles. In the case of I_2^A the four atoms (red spheres) of the "Z structure" replace two neighboring atoms of the ideal lattice, whereas in the case of I_2^C the five atoms of the "W structure" replace three neighbors on the zig-zag line along [1–10]. On the other hand, the three atoms of I_2^B replace one atom of the ideal lattice.

simulations were performed for three different initial configurations (I_2^A, I_2^B, and I_2^C). The simulation time varied between 5 ns (1600 K) and 100 ns (800 K). As expected, the results do not depend significantly on the initial configuration since the simulation time is very long compared to the period after which an initially metastable defect reaches the state of the free energy minimum. In all cases considered, the di-interstitial does not dissociate during the migration. Typical trajectories of the center of mass of the di-interstitial are shown in Fig. 3. At low temperature a high mobility on a zig-zag-like line along a ⟨110⟩ axis is found, whereas the change between equivalent ⟨110⟩ directions occurs seldom and requires a long time. At high temperature a frequent change between equivalent ⟨110⟩ migration directions is observed. The motion on the zig-zag-like trajectory occurs in a {110} plane. The detailed investigation of the atomic mechanisms showed, that during this motion the di-interstitial structure changes continuously between I_2^A and other configurations. Figure 4 illustrates the migration of a di-interstitial within a {110} plane. The configuration I_2^A is clearly visible at three stages. At another stage the di-interstitial has the I_2^C structure. A migration sequence with the I_2^C configuration and a more complex di-interstitial structure is shown in Fig. 5. Figures 4 and 5 demonstrate the variety of the atomic mechanisms of the di-interstitial diffusion. During the migration along the zig-zag-like trajectory, occasionally, the di-interstitial moves out of the {110} plane, and the I_2^B structure is formed. Three atoms of this configuration lie on the edges of a triangle in a {111} plane, a fourth atom is situated outside this plane (cf. Fig. 1 and Table I).

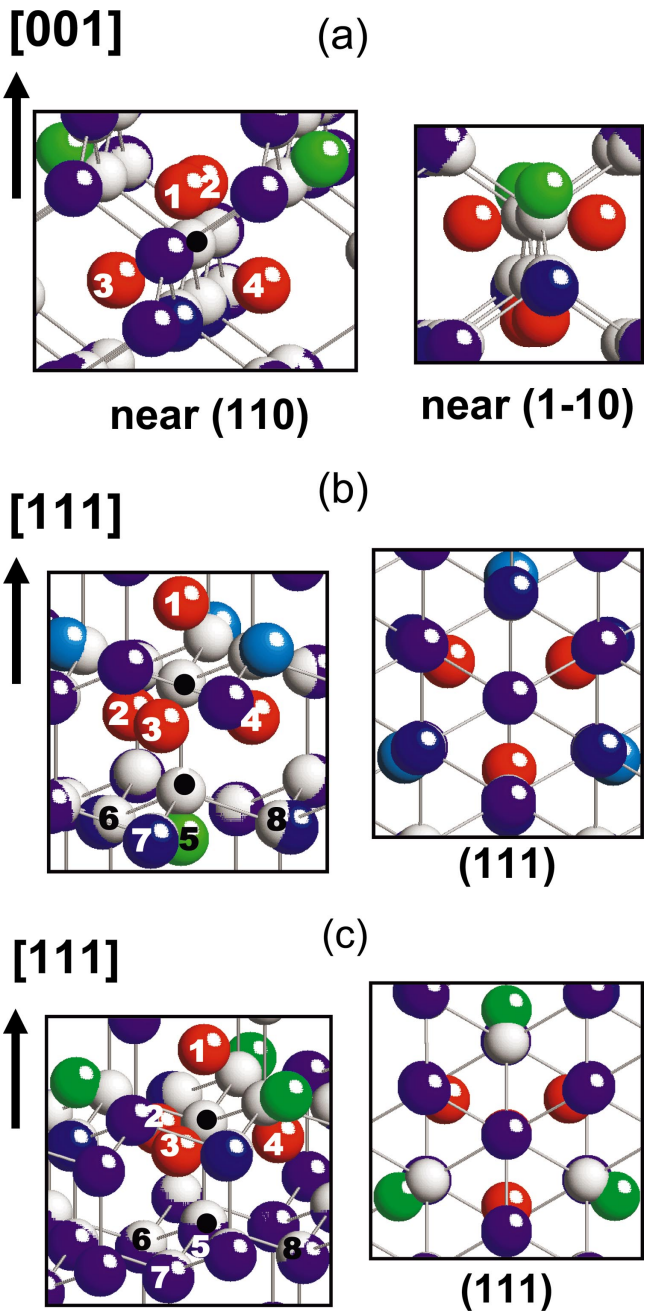

FIG. 2. (Color) The three most stable tri-interstitial structures: I_3^A (a), I_3^B (b), and I_3^C (c). The formation energies are given in Table I. In order to make the comparison with similar configurations found by other authors (Refs. 8, 12–14, and 39) easier, some atoms are numbered. The four atoms of I_3^A (red spheres) belong to the lattice site marked by the black dot. Atoms 1–5 of I_3^B and I_3^C are related to the two lattice sites marked by the black dots.

The I_2^B configuration is immobile. It shows only thermal vibrations and exists over a relatively long period. Thermal fluctuations may lead to the rotation of I_2^B triangle into a {110} plane and to the transformation into I_2^A or another mobile configuration. Then, the di-interstitial migration continues. The transformation from the immobile I_2^B structure to a mobile di-interstitial configuration is illustrated in Fig. 6. This complex process cannot only be reduced to a rigid rotation of the I_2^B triangle from the {111} to the {110} plane. It is characterized by collective atomic rearrangements in the vicinity of the di-interstitial. The transformation from a mobile configuration to I_2^B shows similar features. In a simplified picture, the di-interstitial diffusion can be described by two effective energy barriers: a low barrier for the migration on zig-zag-like trajectories along a ⟨110⟩ direction (and in a {110} plane), and a high barrier for the change between equivalent ⟨110⟩ migration directions (and between equivalent {110} migration planes) via the I_2^B structure. Really, there may exist a number of barriers both for the migration in the {110} plane and for the change between equivalent {110} planes. The diffusivity D_d^{110} of the di-interstitial migration within {110} planes and the rate ω_d^{110} for the change between equivalent {110} migration planes were determined by subdividing the trajectories into segments in which the defect moves in different {110} planes. The results are given in Fig. 7. The effective barrier for the migration within a {110} plane is about 0.20 eV whereas the effective barrier for the change between different {110} planes is more than two times higher (0.46 eV). The value of the former barrier seems to contradict the frequent observation of the I_2^C structure as an intermediate di-interstitial configuration (cf. Fig. 4) since the difference between the formation energies of I_2^A and I_2^C is 0.27 eV (cf. Table I). However, at elevated temperatures one has to compare the free energies of formation instead of the formation energies. The formation entropy of I_2^A and I_2^C may differ in such a manner that difference between the free energies of formation becomes smaller than the difference between the formation energies. Another reason for the apparent discrepancy may be the fact that the diffusion via the transition between I_2^A and I_2^C occurs less frequently than via lower barriers so that the effective barrier becomes 0.20 eV. Figure 8 shows that the total di-interstitial diffusivity $D_d^{\text{di-}I}$ is higher than the self-diffusion coefficient per di-interstitial $D_s^{\text{di-}I}$, i.e., the atomic mobility due to the presence of the defect is lower than the di-interstitial mobility. This can be explained by the fact that within a {110} plane the di-interstitial moves like a wave packet. The atoms belonging to the di-interstitial change continuously and in such a manner, that they are less mobile than the di-interstitial. If the only diffusion mechanism were the motion on a zig-zag-like trajectory within a {110} plane, both the di-interstitial migration and the atomic mobility had the same barrier (cf. Ref. 35), i.e., in the Arrhenius plot the lines for $D_d^{\text{di-}I}(T)$ and $D_s^{\text{di-}I}(T)$ would be parallel. However, as discussed above, the mechanism of di-interstitial diffusion changes with increasing temperature. Therefore, the two barriers differ. The effective migration barrier for the di-interstitial is 0.22 eV and the atomic mobility has an effective barrier of 0.38 eV. The former barrier is nearly equal to that determined for the di-interstitial migration on a zig-zag-like trajectory along a ⟨110⟩ direction within a {110} plane. That means that the overall di-interstitial diffusivity is dominated by this process. The higher barrier for the atomic mobility is closer to that for the change between different {110} migration planes. This is consistent with the observation that the transformation between the immobile I_2^B and mobile di-interstitial configurations is characterized by considerable atomic rearrange-

TABLE I. Energetics (formation energy in eV) of di- and tri-interstitials obtained by: (i) classical potential methods (CP), (ii) tight-binding calculations (TB), and (iii) the density-functional theory (DF). A short description characterizes the different defect configurations and their symmetry. In the second column, the values in the brackets are the binding energies (in eV).

	CP			TB			DF					
di-interstitial	This work	Ref. 4[a],[e]	Ref. 5[b]	Ref. 6	Ref. 7	Ref. 8	Ref. 9	Ref. 10	Ref. 11	Ref. 12	Ref. 13	Ref. 14
I_2^A or "Z structure" (C_{2h})	**6.10 (1.74)**	5.70	6.32	8.00	~5.85						6.46	
I_2^B or "modified triangle in {111}" (C_{1h})	**6.14 (1.70)**										6.46	
I_2^C or "W structure" (C_{2v})	**6.37 (1.47)**			7.70	6.07							
"K (Kim) structure" or "triangle in {111}" (C_{1h})				7.30	5.64	4.91	4.9 - 6.0	5.19	4.96	4.84	5.66	5.76–5.84
"L (Lee) structure" (C_2)								6.17				
"C (Coomer) structure" (C_{1h})								5.12				

	CP			TB			DF			
tri-interstitial	This work	Ref. 4[a],[e]	Ref. 15[c],[e]	Ref. 15[d],[e]	Ref. 8	Ref. 15[e]	Ref. 13	Ref. 12	Ref. 16	Ref. 14
I_3^A or "modified tetrahedron" (C_{2v})	**7.54 (4.22)**	7.08								
I_3^B or "modified bond-centered triple I" (C_{3v})	**7.59 (4.17)**									
I_3^C or "modified bond-centered triple II" (C_{3v})	**7.62 (4.14)**									
"tetrahedron" (D_{2d})			8.85	6.03	6.69	7.83	6.96–7.11	6.05	~6.0	7.27
"bond-centered triple" (C_{3v})								6.09		7.32
"triple at tetrahedral site" (C_{3v})							8.22	7.15		8.67
"complex I" (C_2)							6.33–6.72			
"complex II"(C_3)							7.41			

[a]Original Stillinger-Weber potential (Ref. 21).
[b]Tersoff 3 potential (Ref. 23).
[c]Justo potential (Ref. 32).
[d]Lenosky potential (Ref. 15).
[e]In this reference, the defect structure is not explicitly given.

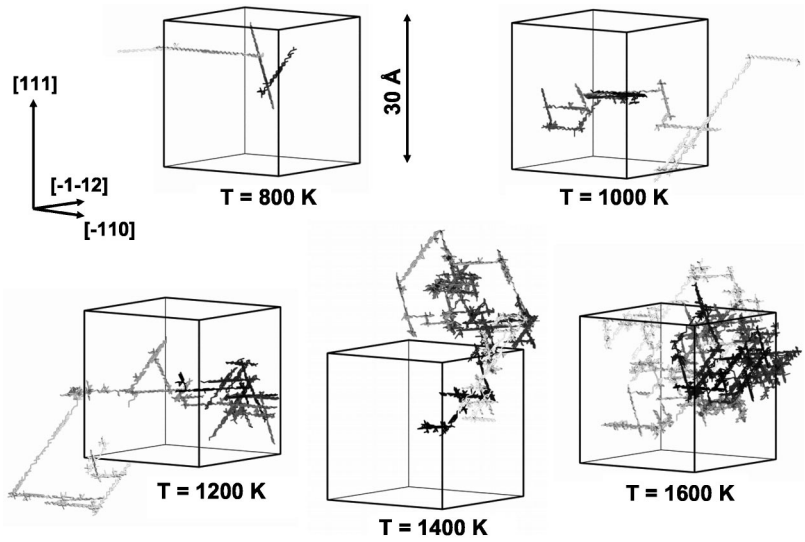

FIG. 3. Trajectories of the center of mass of the di-interstitial at different temperatures, over a period of 4.4 ns. The lines connect positions determined at every tenth time step of the MD simulation. The gray scale is a measure for the migration time. With increasing time, the trajectories become lighter.

ments. It should be mentioned that a similar dependence of the migration mechanisms on the temperature was found for self-interstitial diffusion in metals.[35] Like in the present work, different effective barriers for the defect migration and the atomic mobility were obtained. The temperature dependence of the defect diffusivity and the self diffusion coefficient per defect showed slight deviations from the Arrhenius plot. Such deviations are not clearly visible in Fig. 8. The values of D_d^{110}, ω_d^{110}, $D_d^{\text{di-}I}$, and $D_s^{\text{di-}I}$, as shown in Figs. 7 and 8, were obtained by averaging over the corresponding data determined from simulations with the three different initial configurations I_2^A, I_2^B, and I_2^C. The effective barriers and the pre-exponential factors are summarized in Table II.

The tri-interstitial migration was studied for 1300, 1400, 1500, and 1600 K. The initial defect structures were I_3^A and I_3^B, and the simulation time varied between 15 ns (1600 K) and 100 ns (1300 K). Like in the case of di-interstitial diffusion, the difference between the results obtained for the two start configurations is only due to thermal fluctuations. Characteristic trajectories of the tri-interstitial are depicted in Fig. 9. They indicate that at all temperatures considered the diffusion mechanisms are similar. The tri-interstitial does not migrate within preferred planes like the di-interstitial. A characteristic feature is the migration of the center of mass of the tri-interstitial on complex trajectories around the six-member rings. An example is depicted in the inset of Fig. 9, for $T = 1400$ K. The visual analysis of the atomic rearrangements reveals complex migration mechanisms. Figure 10 shows an example where the center of mass of the tri-interstitial moves around a half of a six-member ring. In the first stage [Figs. 10(a)–10(g)] the center of mass stays approximately within a {110} plane. It is characterized by a continuous change between the I_3^A and the I_3^B configurations. The simplest migration mechanism consists in the exchange of one atom during the transformation $I_3^B \rightarrow I_3^A \rightarrow I_3^B$ [Figs. 10(a)–10(c)]. However, the next transition $I_3^B \rightarrow I_3^A \rightarrow I_3^B$ occurs via a more complex process characterized by a high atomic mobility [Figs. 10(c)–10(g)]. In a simplified manner, it may be described by the exchange of one atom and a rotation of the bond-centered

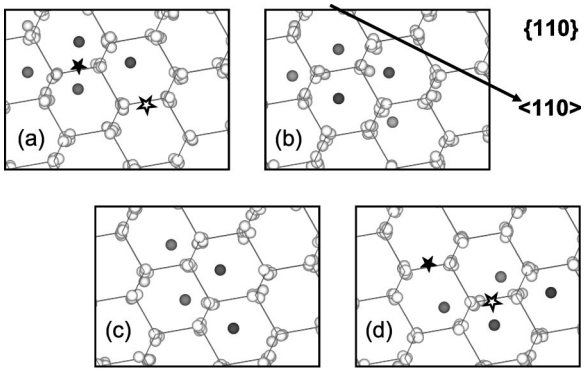

FIG. 4. Details of the di-interstitial migration in a {110} plane ($T = 1200$ K). The lines depict the bonds in the ideal lattice. The spheres show the atoms in the real lattice. Their gray scale is a measure for the deviation of the atomic positions from the ideal lattice sites. With increasing deviation the spheres become darker. The I_2^A configuration is clearly visible in (a), (c), and (d), whereas (b) shows the I_2^C structure. Note that the atoms belonging to the di-interstitial change continuously. For example, from stage (c) to stage (d), one atom of the upper dumbbell is exchanged. The positions of the center of mass of the di-interstitial at the beginning and the end of the migration sequence shown in this figure are marked by filled and open asterisks, respectively. The period between stage (a) and (d) is about 2 ps.

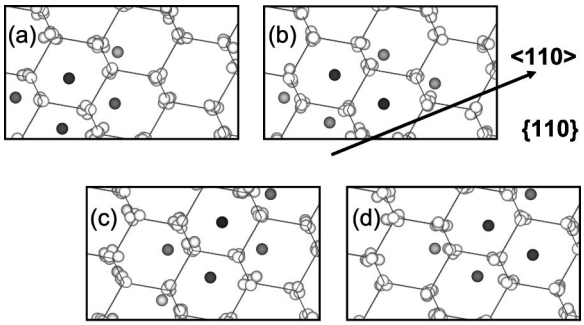

FIG. 5. A complex atomic mechanism of di-interstitial migration ($T = 1200$ K). The I_2^C structure as well as a more complex planar configuration are visible. The period between stage (a) and (d) is about 1 ps.

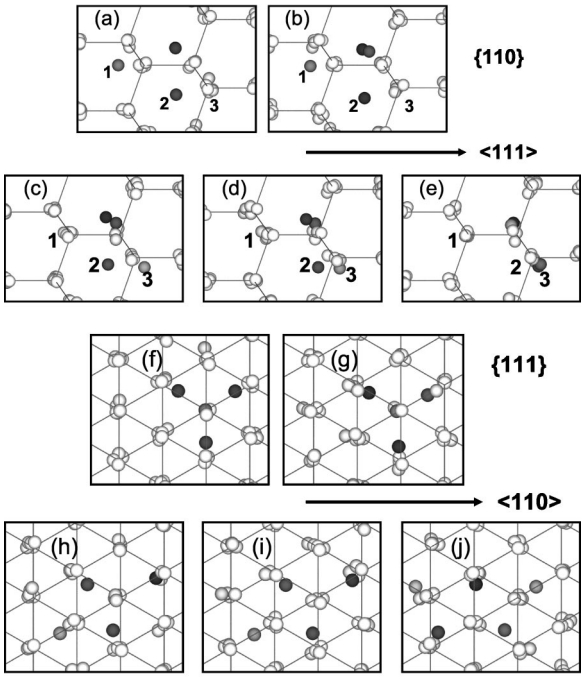

FIG. 6. Transformation from the immobile I_2^B structure to a mobile di-interstitial configuration, over a period of about 1 ps ($T = 1200$ K). Five stages of this process are illustrated in two different views. Figures (a–b) and (f–g) show the I_2^B configuration with its mean feature, the triangle in a {111} plane. The dumbbell formed by the two upper atoms of the triangle rotates into a {110} plane [(b–e) and (g–j)] and, simultaneously, the rearrangement of three other atoms occurs. The latter atoms are marked by numbers. The final di-interstitial configuration lies in the {110} plane perpendicular to the plane of (a)–(e). The structure depicted in (e) and (j) is an intermediate configuration between I_2^A and I_2^C.

triangle. In the second stage [Figs. 10(g)–10(j)] the center of mass of the tri-interstitial moves out of the previous {110} plane. The present example shows a high atomic mobility and very complex structures during this transition. Finally,

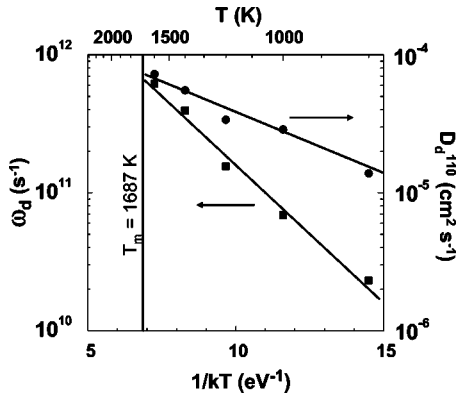

FIG. 7. The diffusivity D_d^{110} for the di-interstitial migration within {110} planes and the rate ω_d^{110} for the change between equivalent {110} migration planes in dependence on the temperature. The barriers and the pre-exponential factors obtained for both quantities are given in Table II.

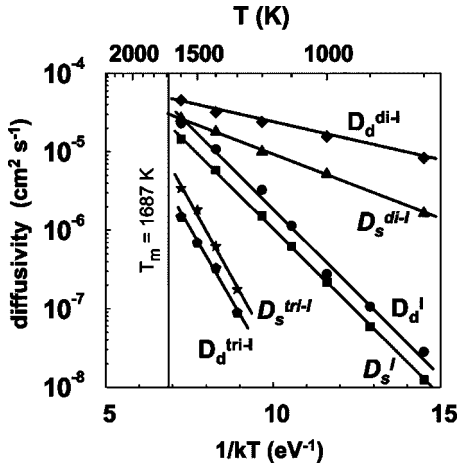

FIG. 8. Defect diffusivities and self-diffusion coefficients per defect for the mono-, the di-, and the tri-interstitial. The values for the effective migration barriers and the pre-exponential factors are given in Table II.

the center of mass reaches a plane parallel to the former {110} plane, and a transformation $I_3^A \rightarrow I_3^B$ takes place [Figs. 10(j) and 10(k)]. Despite the complex and extended intermediate configurations found throughout the tri-interstitial diffusion, a complete dissociation was never observed. Figure 8 shows the tri-interstitial diffusivity $D_d^{\text{tri-}I}$ and the self-diffusion coefficient $D_s^{\text{tri-}I}$ per tri-interstitial versus reciprocal temperature. The barriers for the atomic mobility and the defect migration are about 1.8 and 1.7 eV, respectively. In contrast to the di-interstitial, the atoms are more mobile than the defect. This can be explained by the complex and frequent rearrangements of atoms observed during the tri-interstitial migration. The effective barriers and the pre-exponential factors for the tri-interstitial diffusion are given in Table II.

Using a simulation cell with $2880+2$ atoms for the di-interstitial, and with $5040+3$ atoms for the tri-interstitial, the influence of the cell size on the results of di- and tri-interstitial migration was investigated for one start configuration and one temperature. The data obtained do not show a significant size dependence. However, test calculations demonstrated that in the case of the di-interstitial migration the use of a simulation cell with less than 500 atoms may lead to wrong results due to the interaction between the defect and its periodic replicas.

Figure 8 depicts also the results obtained from migration simulations for the mono-interstitial. D_s^I and D_d^I are smaller than the corresponding values for the di-interstitial, but higher than those for the tri-interstitial. The barriers for the atomic mobility and the defect diffusion lie between those for the di- and the tri-interstitials as well. The fact that the both barriers are equal (0.98 eV) indicates that the migration mechanism does not change with temperature. Like in the case of the di-interstitial, the defect diffusivity is higher than the self-diffusion coefficient per defect. The data for the mono-interstitial are summarized in Table II. The values for D_s^I and D_d^I were obtained for temperatures between 800 and 1600 K. The simulation time varied between 5 ns (1600 K) and 500 ns (800 K).

TABLE II. Values for the effective migration barrier and the pre-exponential factor of the quantities shown in the Arrhenius plots in Figs. 7 and 8. D_d^{110} is the diffusivity for the di-interstitial migration within {110} planes and ω_d^{110} is the rate for the change between equivalent {110} planes. D_d and D_s denote the defect diffusivity and the self-diffusion coefficient per defect.

	D_d^{110}		ω_d^{110}		D_d		D_s	
Defect	E_m(eV)	D_0(cm^2 s^{-1})	E_m(eV)	ω_0(s^{-1})	E_m(eV)	D_0(cm^2 s^{-1})	E_m(eV)	D_0(cm^2 s^{-1})
di-interstitial	0.20 ± 0.05	$(2.9\pm0.6)\times10^{-4}$	0.46 ± 0.10	$(1.9\pm0.4)\times10^{13}$	0.22 ± 0.04	$(2.2\pm0.4)\times10^{-4}$	0.38 ± 0.03	$(4.1\pm0.6)\times10^{-4}$
tri-interstitial					1.7 ± 0.3	0.34 ± 0.2	1.8 ± 0.2	1.4 ± 0.5
mono-interstitial					0.98	0.035	0.98	0.019

Recent theoretical investigations found a relatively high mobility of the di- and the tri-interstitials as well. In the first MD study on di-interstitial migration, Gilmer *et al.*[4] obtained a barrier of about 0.2 eV for the atomic mobility. In their investigations with the original SW potential[21] they did not determine the di-interstitial diffusivity. Marques *et al.*[5] employed the Tersoff 3 potential[23] and found also a high mobility of the di-interstitial, but they did not calculate the diffusivity. Using the Tersoff potential Kapur *et al.*[17] investigated the diffusion of clusters containing one to nine self-interstitials at $T=2650$ K. The cluster diffusivity decreases monotonically with increasing cluster size. This is in contrast to the results of the present work. However, the data of Kapur *et al.*[17] should be treated with caution since many authors found that the melting temperature for the Tersoff potential is below 2650 K.[5,24,30,31] Using tight-binding MD simulations Hane *et al.*[7] obtained a barrier of about 1.3 eV for the atomic mobility during di-interstitial migration, whereas Kim *et al.*[9] found a barrier of about 0.7 eV for the di-interstitial migration. Recent long-time tight-binding MD simulations of Richie *et al.*[13] yielded a barrier of about 0.5 eV both for di- and tri-interstitial migration. A high mobility of di- and tri-interstitials was also found by Estreicher *et al.*[18] using density-functional-theory MD for short periods. In particular they described a migration mechanism for the tri-interstitial which is very similar to that shown in Figs. 10(a)–10(c). The migration barriers of the defects were also

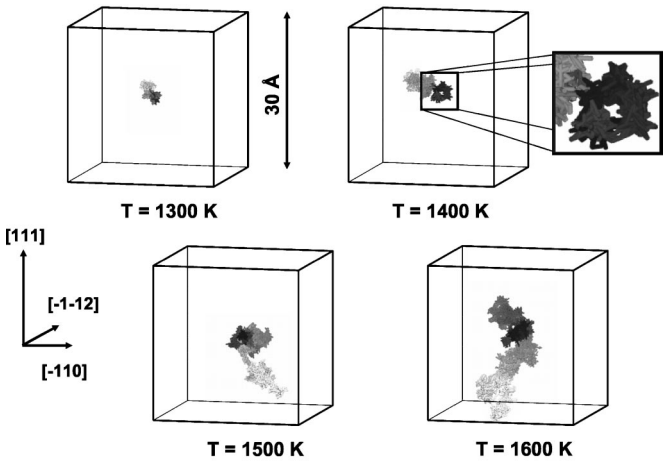

FIG. 9. Trajectories of the tri-interstitial over a period of 14.4 ns, at 1300, 1400, 1500, and 1600 K. The presentation is similar to Fig. 3. For $T=1400$ K, the inset depicts complex trajectories around a six-member ring.

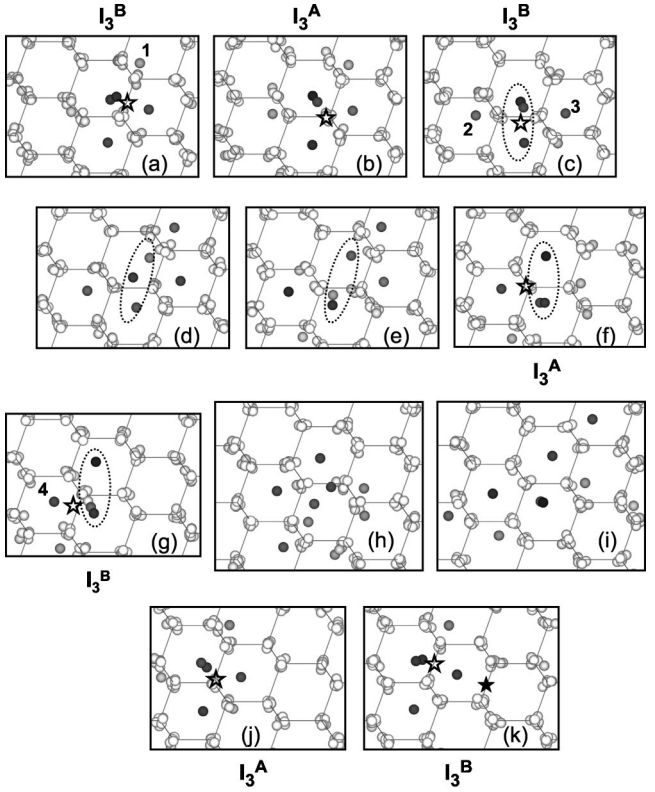

FIG. 10. Migration of the tri-interstitial around a half of a six-member ring, over a period of about 35 ps ($T=1600$ K). The presentation is similar to Figs. 4–6. The approximate position of the center of mass of the tri-interstitial is marked by the open asterisks. For comparison, the filled asterisk in (k) shows the center of mass at the beginning of the migration sequence (a). In the first stage, the tri-interstitial moves within a {110} plane [(a)–(g)]. The simplest migration mechanism is the exchange of atom 1 by atom 2 during the transformation $I_3^B \rightarrow I_3^A \rightarrow I_3^B$ [(a)–(c)]. The next transition $I_3^B \rightarrow I_3^A \rightarrow I_3^B$ is a more complex process with a high atomic mobility [(c)–(g)]. In a simplified manner, it may be described by the exchange of atom 3 by atom 4 and a rotation of the bond-centered triangle marked by the dotted ellipse. In the second stage [(g)–(j)] the center of mass of the tri-interstitial moves out of the previous {110} plane. The present example shows a high atomic mobility and very complex structures during this transition [(h)–(i)]. Finally, the center of mass reaches a plane parallel to the former {110} plane, and the transformation $I_3^A \rightarrow I_3^B$ takes place [(j)–(k)].

estimated by static potential energy considerations which are based on the density-functional theory. For the di-interstitial a value of 0.5 eV was obtained whereas the barrier determined for the tri-interstitial is 0.75 eV.[19] Very recently, Du *et al.*[20] found a value of 0.5 eV for the migration barrier of the tri-interstitial.

A comparison of the theoretical results on the migration of mono-, di-, and tri-interstitials with measurements is very difficult since the defect diffusivities can be only obtained by a rather complex theoretical analysis of the experimental data. The first class of experiments concerns the defect evolution and the transient-enhanced diffusion of boron during post-implantation annealing. The successful theoretical description[1–3] of these effects is based on a number of assumptions. The following are related to the subject of the present work: (i) During ion implantation only mono-interstitials and mono-vacancies are formed. Their concentration is much higher than in the thermodynamic equilibrium. (ii) The mono-interstitial and the mono-vacancy are the only mobile intrinsic defects. They recombine or form immobile clusters. In particular self-interstitial clusters—amongst them the di- and the tri-interstitial—are introduced to obtain a transient storage of self-interstitials and to explain the formation of {311} defects and dislocation loops. On the other hand, there is no experimental evidence against a mobility of di- and tri-interstitials. Recently, Martin-Bragado *et al.*[42] presented a first attempt to include the di-interstitial as a mobile species. They concluded that this assumption may lead to some changes in the theoretical interpretation of the experimental data. Furthermore, the assumption that mono-interstitials and mono-vacancies are the only as-implanted defects is too simple. Atomistic computer simulations showed[43–45] that various complex defects are formed within several picoseconds after ion impact. Amongst these defects, di-interstitials could be identified.[46] Obviously, there exists two channels to form di- and tri-interstitials: (i) the direct formation after the fast relaxation within the regions of collision cascades, and (ii) the agglomeration of mono-interstitials controlled by diffusion and reaction processes. These results are important for the discussion of a second class of experiments. In these investigations a long-range, trap-limited migration of implantation-induced self-interstitial defects was found at room temperature.[47–49] Assuming that these defects are mobile mono-interstitials, the theoretical analysis of the experimental data led to lower bounds for their diffusivity. Kyllesbech Larsen *et al.*[47] and Privitera *et al.*[48] found a value of about 10^{-11} cm^2 s^{-1}, whereas Collart *et al.*[49] obtained 10^{-7} cm^2 s^{-1} using *in situ* measurements. However, these values are about twenty orders of magnitude larger than the diffusivity obtained by diffusion experiments near the thermodynamic equilibrium.[50–53] They are also much larger than the mono-interstitial diffusivity used in the interpretation of defect evolution and transition-enhanced diffusion of boron during post-implantation annealing[1,2] and larger than many theoretical results.[13,27,54] On the other hand, the experimental data may be interpreted by assuming di-interstitial migration since the present work yields a di-interstitial diffusivity of about 5×10^{-8} cm^2 s^{-1} at room temperature. For reasons given in the following, this explanation is supported by two observations: (i) the defect injection occurs immediately after the implantation has started,[49] and (ii) the interstitial-like defects contributing to the long-range migration are only a very small fraction of the implantation damage.[47,48] As mentioned above, atomistic studies demonstrated that di-interstitials are part of the as-implanted defect structure formed within several picoseconds after the ion impact.[46] Compared to the total amount of defects, their number is low. Furthermore, only a small percentage of the formed di-interstitials should be able to escape from the region of implantation damage and become freely migrating defects. The latter argument is consistent with the observation that the efficiency of defect injection decreases with the implantation dose.[47,49] An alternative explanation for the observed effects might be the ionization-enhanced mobility of the mono-interstitial, an effect known from electron irradiation at low temperatures.[55] However, since the defect migration occurs also far outside the implanted region this interpretation seems to be not realistic.[47]

IV. CONCLUSIONS

The migration of di- and tri-interstitials has been investigated by a comprehensive atomistic study. In order to test the accuracy of the interatomic potential used, before the migration simulation the structure and energetics of di- and tri-interstitials have been determined. The results are comparable with those of tight-binding and density-functional-theory calculations.

Starting with one of the most stable defect configurations, the migration of di- and tri-interstitials has been investigated for temperatures between 800 and 1600 K. In comparison with the mono-interstitial, the di-interstitial migrates faster, whereas the tri-interstitial has a lower diffusivity. The mobility of the di-interstitial is higher than the mobility of the lattice atoms during the defect migration. On the other hand, the tri-interstitial migration is slower than the corresponding atomic diffusion. The mechanism of di-interstitial diffusion depends on the temperature. This is due to the significant difference between the barriers for the di-interstitial migration within {110} planes and for the change between equivalent {110} migration planes. The former barrier is nearly equal to the effective barrier of the total diffusivity of the di-interstitial, whereas the latter barrier is closer to that of the self-diffusion coefficient per di-interstitial. This indicates that the overall di-interstitial diffusivity is dominated by the migration within the {110} planes, and that the atomic mobility has its maximum during the change between equivalent {110} migration planes. The di-interstitial structures I_2^A and I_2^C were identified as mobile configurations whereas I_2^B is immobile. The atomic mechanisms of the migration of tri- and mono-interstitials are independent of temperature. The tri-interstitial diffusion is characterized by frequent rearrangements of atoms. Therefore the atomic mobility is higher than that of the tri-interstitial. The comparison of the results of the systematic study performed in this work with the few literature data on di- and tri-interstitial migration does not lead to a unique picture. However, the most authors found also an effective migration barrier for the di-interstitial far below 1 eV.

A relatively high mobility of di- and tri-interstitials may have implication for the current understanding of the results of many experimental investigations performed in the last decade. In particular a revision of the interpretation of experiments on defect evolution and transient-enhanced diffusion of boron may be necessary. Furthermore, the implantation-induced migration of interstitial-like defects observed at room temperature may be explained by the diffusion of di-interstitials.

ACKNOWLEDGMENTS

M.P. would like to thank Dr. H. Bracht, University of Münster, Germany, for helpful discussions.

*FAX: +49 351 260 3285. Electronic address: M.Posselt@fz-rossendorf.de

[1] N. E. B. Cowern, G. Mannino, P. A. Stolk, F. Roozeboom, H. G. A. Huizing, J. G. M. vanBerkum, F. Cristiano, A. Claverie, and M. Jaraiz, Phys. Rev. Lett. **82**, 4460 (1999).
[2] L. Pelaz, M. Jaraiz, G. H. Gilmer, H.-J. Gossmann, C. S. Rafferty, D. J. Eaglesham, and J. M. Poate, Appl. Phys. Lett. **70**, 2285 (1997).
[3] P. Pichler and D. Stiebel, Nucl. Instrum. Methods Phys. Res. B **186**, 256 (2002).
[4] G. H. Gilmer, T. Diaz de la Rubia, D. M. Stock, and M. Jaraiz, Nucl. Instrum. Methods Phys. Res. B **102**, 247 (1995).
[5] L. A. Marques, L. Pelaz, J. Hernandez, J. Barbolla, and G. H. Gilmer, Phys. Rev. B **64**, 045214 (2001).
[6] P. B. Rasband, P. Clancy, and M. O. Thompson, J. Appl. Phys. **79**, 8998 (1996).
[7] M. Hane, T. Ikezawa, and G. H. Gilmer, in *Proceedings of the International Conference on Simulation of Semiconductors Processes and Devices* (IEEE, Piscataway, 2000), p. 119.
[8] A. Bongiorno, L. Colombo, F. Cargnoni, C. Gatti, and M. Rosati, Europhys. Lett. **50**, 608 (2000).
[9] J. Kim, F. Kirchhoff, W. G. Aulbur, J. W. Wilkins, F. S. Khan, and G. Kresse, Phys. Rev. Lett. **83**, 1990 (1999).
[10] R. Jones, T. A. G. Eberlein, N. Pinho, B. J. Coomer, J. P. Goss, P. R. Briddon, and S. Öberg, Nucl. Instrum. Methods Phys. Res. B **186**, 10 (2002).
[11] M. P. Chichkine, M. M. DeSouza, and E. M. S. Sankara Narayanan, Phys. Rev. Lett. **88**, 085501 (2002).
[12] M. P. Chichkine and M. M. DeSouza, Phys. Rev. B **66**, 045205 (2002).
[13] D. A. Richie, J. Kim, S. A. Barr, K. R. A. Hazzard, R. Hennig, and J. W. Wilkins, Phys. Rev. Lett. **92**, 045501 (2004).
[14] G. M. Lopez and V. Fiorentini, Phys. Rev. B **69**, 155206 (2004).
[15] T. J. Lenosky, B. Sadigh, E. Alonso, V. V. Bulatov, T. Diaz de la Rubia, J. Kim, A. F. Voter, and J. D. Kress, Modell. Simul. Mater. Sci. Eng. **8**, 825 (2000).
[16] J. Kim, F. Kirchhoff, J. W. Wilkins, and F. S. Khan, Phys. Rev. Lett. **84**, 503 (2000).
[17] S. S. Kapur, M. Prasad, and T. Sinno, Phys. Rev. B **69**, 155214 (2004).
[18] S. K. Estreicher, M. Gharaibeh, P. A. Fedders, and P. Ordejon, Phys. Rev. Lett. **86**, 1247 (2001).
[19] T. A. G. Eberlein, N. Pinho, R. Jones, B. J. Coomer, J. P. Goss, P. R. Briddon, and S. Öberg, Physica B **308-310**, 454 (2001).
[20] Y. Du, R. G. Hennig, and J. W. Wilkins, Abstract C 6.2, MRS Spring Meeting 2004, April 12–16, 2004, San Francisco, CA.
[21] F. H. Stillinger and T. A. Weber, Phys. Rev. B **31**, 5262 (1985).
[22] H. Balamane, T. Halicioglu, and W. A. Tiller, Phys. Rev. B **46**, 2250 (1992).
[23] J. Tersoff, Phys. Rev. B **38**, 9902 (1988).
[24] S. J. Cook and P. Clancy, Phys. Rev. B **47**, 7686 (1993).
[25] *Properties of Silicon*, edited by R. Hull Vol. 20 in Emis Datareviews Series (INSPEC, London, 1999).
[26] H. R. Schober, Phys. Rev. B **39**, 13013 (1989).
[27] L. Colombo, Annu. Rev. Mater. Res. **32**, 271 (2002).
[28] O. K. Al-Mushadani and R. J. Needs, Phys. Rev. B **68**, 235205 (2003).
[29] M. I. J. Probert and M. C. Payne, Phys. Rev. B **67**, 075204 (2003).
[30] P. J. Ungar, T. Halicioglu, and W. A. Tiller, Phys. Rev. B **50**, 7344 (1994).
[31] K. Nordlund and R. S. Averback, Phys. Rev. B **56**, 2421 (1997).
[32] J. F. Justo, M. Z. Bazant, E. Kaxiras, V. V. Bulatov, and S. Yip, Phys. Rev. B **58**, 2539 (1998).
[33] H. J. C. Berendsen, J. P. M. Postma, W. F. van Gunsteren, A. DiNola, and J. R. Haak, J. Chem. Phys. **81**, 3684 (1984).
[34] J. C. Noya, C. P. Herrero, and R. Ramirez, Phys. Rev. B **53**, 9869 (1996).
[35] Yu. N. Osetsky, Defect Diffus. Forum **188-190**, 71 (2001).
[36] J. Marian, B. D. Wirth, A. Caro, B. Sadigh, G. R. Odette, J. M. Perlado, and T. Diaz de la Rubia, Phys. Rev. B **65**, 144102 (2002).
[37] Yu. N. Osetsky, D. J. Bacon, A. Serra, B. N. Singh, and S. I. Golubov, Philos. Mag. **83**, 61 (2003).
[38] M. W. Guinan, R. N. Stuart, and R. J. Borg, Phys. Rev. B **15**, 699 (1977).
[39] M. Gharaibeh, S. K. Estreicher, and P. A. Fedders, Physica B **273-274**, 532 (1999).
[40] Y. H. Lee, N. N. Gerasimenko, and J. W. Corbett, Phys. Rev. B **14**, 4506 (1976).
[41] Y. H. Lee, Appl. Phys. Lett. **73**, 1119 (1998).
[42] I. Martin-Bragado, M. Jaraiz, P. Castrillo, R. Pinachio, J. Barbolla, and M. M. De Souza, Phys. Rev. B **68**, 195204 (2003).
[43] M. J. Caturla, T. Diaz de la Rubia, L. A. Marques, and G. H. Gilmer, Phys. Rev. B **54**, 16683 (1996).
[44] K. Nordlund, M. Ghaly, R. S. Averback, M. Caturla, T. Diaz de la Rubia, and J. Taurus, Phys. Rev. B **57**, 7556 (1998).
[45] M. Posselt, Mater. Res. Soc. Symp. Proc. **647**, O2.1.1 (2001).
[46] M. Posselt (unpublished).
[47] K. Kyllesbech Larsen, V. Privitera, S. Coffa, F. Priolo, S. U. Campisano, and A. Carnera, Phys. Rev. Lett. **76**, 1493 (1996).
[48] V. Privitera, S. Coffa, F. Priolo, K. Kyllesbech Larsen, and G. Mannino, Appl. Phys. Lett. **68**, 3422 (1996).
[49] E. J. H. Collart, K. Weemers, N. E. B. Cowern, J. Politiek, P. H. L. Bancken, J. G. M. van Berkum, and D. J. Gravesteijn, Nucl. Instrum. Methods Phys. Res. B **139**, 98 (1998).

[50] H. Bracht, N. A. Stolwijk, and H. Mehrer, Phys. Rev. B **52**, 16542 (1995).
[51] A. Giese, H. Bracht, N. A. Stolwijk, and D. Baither, Mater. Sci. Eng. B **71**, 160 (2000).
[52] H. Bracht, E. E. Haller, and R. Clark-Phelps, Phys. Rev. Lett. **81**, 393 (1998).
[53] H. Bracht, J. F. Pedersen, N. Zangenberg, A. N. Larsen, E. E. Haller, G. Lulli, and M. Posselt, Phys. Rev. Lett. **91**, 245502 (2003).
[54] M. Tang, L. Colombo, J. Zhu, and T. Diaz de la Rubia, Phys. Rev. B **55**, 14279 (1997).
[55] G. D. Watkins, in *Radiation Effects in Semiconductors*, edited by F. L. Vook (Plenum, New York, 1968), p. 67.